Opto-Electronic Engineering

Article

2017, Vol 44, Issue 1

In-band metamaterial cloak based on the interplay of absorption and transmission

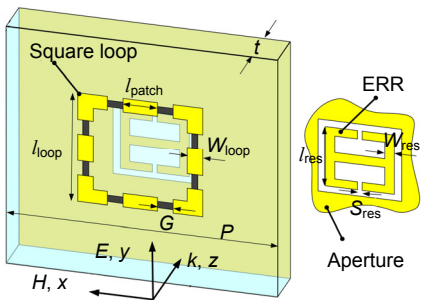

Zeyu Zhao and Hongbo Sun*

State Key Laboratory on Integrated Optoelectronics, College of Electronic Science and Engineering, Jilin University, Changchun 130012, China

Abstract: A microwave metamaterial shelter with an electromagnetic narrow window over a broad absorption spectrum is experimentally demonstrated by resorting to conventional impedance-matching theory and metamaterial resonance. This device consists of a broad absorber and an embedded electric resonator, and has the ability of permitting one to "see" surroundings but not to be readily sensed by outside detectors. The origin is verified to be a dipole oscillation excited in absorbing region which can induce selective re-emission of the captured energy towards the enclosed space. The performance of "observing without being perceived" is numerically presented.

Keywords: metamaterial; cloak; absorption

DOI: 10.3969/j.issn.1003-501X.2017.01.010 **Citation:** *Opto-Elec Eng*, 2017, **44**(1): 92–96

1 Introduction

Over last several decades, the quest for electromagnetic "invisibility" that ever occurred in myths and films only, has always been a research hot topic and maintained the capability of drawing intense interest of microwave engineers. In this field, one conventional approach is that utilizing material with high absorbance to cover a scattering object, and then absorbing incident wave as possible to obtain low-echo effect[1–3]. Recently, another concept manipulating the electromagnetic field based on transformation optics[4], conformal mapping[5] and virtual shaping[6-7] was proposed as an enhanced solution at microwave[8], terahertz[9] and optical frequencies[10-11]. In this case, incident wave is bent around an object by a cloak with specified electromagnetic parameters, permitting outside observers to "see through and behind" the cloaked region without noticing the presence of the object. Based on the photonic spin-orbit interaction[12-15], the bandwidth of virtual shaping can be greatly increased. Indeed, both the absorbing and shaping technologies are effective to make a scattering object un-identified or "unseen". However, "observing without being perceived" in electromagnetic field, meaning invisibility and simultaneously keeping a lookout over outside world analogous to what Harry Potter did in his cloak, has inspired human's enduring enthusiasm for centuries to aspire after but not experimentally realized so far.

One-facet invisibility has already been well developed from Salisbury absorbing screen to the recently proposed metamaterial (MM) cloak devices. Yet, they are not available as choice for shading an internal object, such a detector which needs to keep a lookout over and electromagnetic communication with outside world. The reason is that although absorber can dramatically capture impinging energy and has already achieved engineering applications[16], perfect absorption would result in an electromagnetically isolated space. Without exception, cloaking technique also encounters the analogous embarrassment. A typical cloak, in principle, does not allow the incident wave to enter the enclosed space.

For ideally shading a detector, the issue naturally coming into sights, as described in Fig. 1(a), is that would it be possible to avoid one positioned in the shaded area to be blind at a specified frequency, but still keep enough invisibility performance in a wide frequency range? To address this question, what needs to be realized is to make the external field be able to enter the enclosed region by some means or other, rather than transforming field round the object or exhausting them in the form of heat. Recently, "scattering cancellation" effect[17] is shown to theoretically realize the purpose of "cloaking a sensor"[18]. However, this method would cause a strong unwanted scattering source nearby the original scattering peak of internal dipole owing to the unavoidable plasmonic resonance of shell at the negative permittivity

Received 3 October 2016; accepted 16 December, 2016
* E-mail: John116@126.com

point. Here, by utilizing MM resonator[19-20], we experimentally show a solution by constructing a shelter with an electromagnetic narrow window located in a broad low-echo band at microwave frequencies. This device has the ability of obvious broad scattering reduction through absorbing incident wave, and simultaneously keeps a covered detector workable through re-emitting a portion of the captured energy towards the enclosed space, thus indicating great potentials for unperceived detecting.

2 Design and experimental validation

Fig. 1(b) schematically demonstrates the unit-cell of the MM shelter. It is composed of two basic elements: a metallic square-loop with two small gaps in each side, and an electric-resonant-ring(ERR) embedded into a sub-wavelength aperture. Then, eight chip-resistors are respectively inserted into the gaps of square-loop to provide necessary lossy source. Fig. 2(a) separately shows the images of the MM shelter, ERR layer, and square-loop layer with chip-resistors. Periodic ERR array, containing 20×20 units, is patterned on a 0.82 mm-thick Rogers RO4003 board. In an analogous way, metallic square-loop array is also printed, and 3200 (8×400) chip-resistors with resistance about 80 ohms (tolerance of 5%) are loaded into the gaps using surface-mounting techniques. Subsequently, two boards are assembled together to obtain the sample consisting of loop-RO4003-Air-RO4003-ERR.

In our structure, the metallic square-loop inserted with chip-resistors dominates the broad low-echo characteristic. When incident wave has the corresponding propagation and polarization directions indicated in Fig. 1(b), we can calculate the effective impedance

$$Z_{\text{loop}} = 1/(\mathrm{j}\omega C_{\text{sepa}} + 1/(R + \mathrm{j}\omega L_{\text{loop}})) \quad , \qquad (1)$$

in which the inductance L_{loop} and resistance R are respectively and mainly provided by the side of square-loop parallel with incident electric field and the eight inserted chip-resistors, the capacitance C_{sepa} is formed between

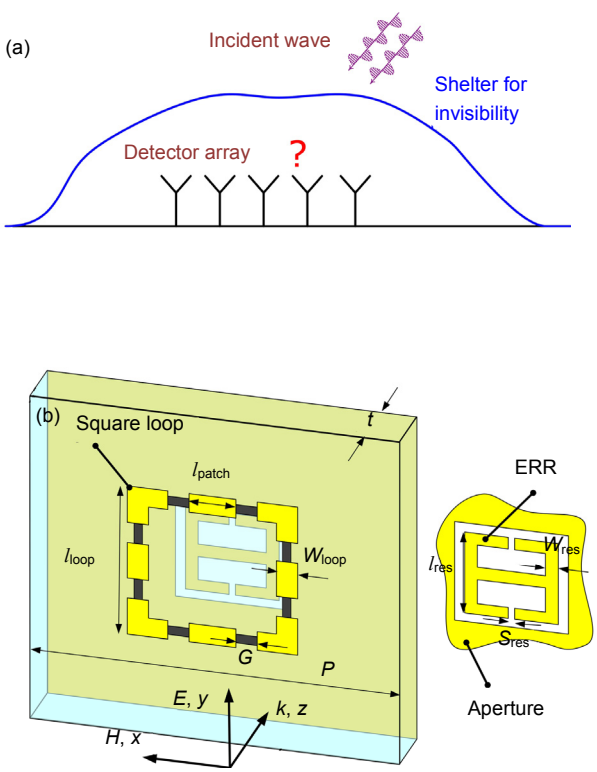

Fig.1 (a) Detector array is out-of-function when covered by electromagnetic cloak or conventional absorber. (b) Schematic drawings of a meta-material shelter with an in-band electromagnetic transparent window. The black sticks represent chip-resistors. The propagation and polarization directions are indicated in (b) with axes and respective dimension notations are listed correspondingly.

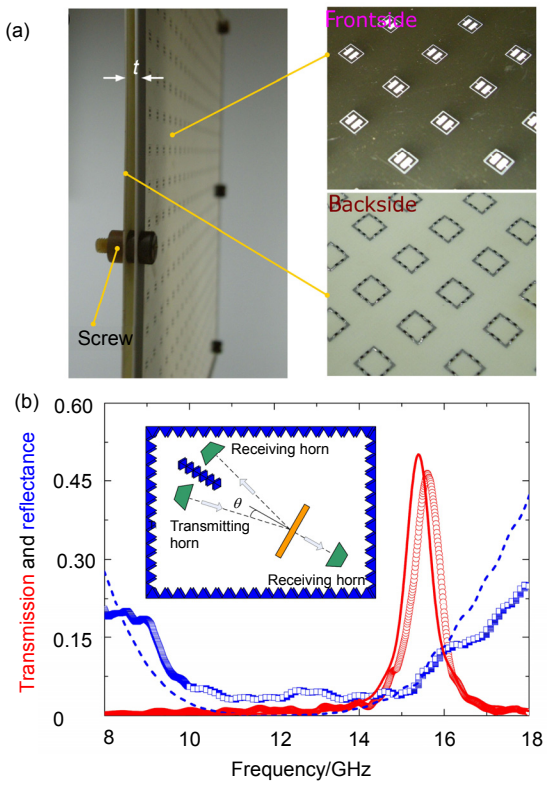

Fig.2 (a) Photographs of the MM shelter (Left), ERR layer (Right and up), and square-loop layer (Right and down) with chip-resistor. (b) Simulated and measured $T(\omega)$ (simulation: solid line, Measurement: circle, red) and $R(\omega)$ (simulation: dash line, measurement: square, blue). The inset picture shows the method of the sample measurement. All equipments are located into an environment decorated with radar absorbing materials. The normal $R(\omega)$ is approximated by the oblique one with a small angle (θ=5 degree). The coupling between transmitting and receiving horns is obstructed by placing high absorption materials between them.

the metal portion of the aperture and square-loop. By optimizing R, the relevant geometric parameters, such as the loop's length L_{loop} and width W_{loop}, following the principle of dispersion engineering[21-25], wideband impedance-matching with outside space can be reached to ensure the incident field entering the interior region of the MM shelter. In this way, behaving analogous with conventional circuit analogy absorber and recently proposed MM absorber [22,26-28], the captured energy can be completely converted into heat by Ohmic losses of metal and the chip-resistors, resulting in near-zero reflectance over a wide frequency range. Another main component, ERR embedded into subwavelength aperture, plays a key role to open an electromagnetic transparent window at an interest frequency. A strong dipole response is excited when ERR interacts with the electric field in the internal region of MM shelter. This dipole oscillation can prevent a portion of energy to be converted into heat by re-emitting it out directionally through the subwavelength aperture, while the backward emission is blocked to maintain the low-echo characteristic.

A vector network analyzer (No. ZVA40-RS) is utilized to characterize the MM shelter. The transmission $T(\omega)$ and reflectance $R(\omega)$ are presented in Fig. 2(b). The measured sample has optimized dimensions, in millimeters, of: P=11.8, l_{loop}=5.6, W_{loop}=0.5, G=0.8, l_{patch}=0.8, D=3.7, l_{res}=3.5, W_{res}=0.6, S_{res}=0.1, t=0.4. For the case of y-polarization (the electric field is perpendicular with the split-wire), we observe that $R(\omega)$ is drastically suppressed in a wide frequency range. $T(\omega)$ is near-zero in almost all frequency points, except a sharp peak with value up to 50% and relative bandwidth of 4.7% at about 15.4 GHz in low-reflectance band, showing that a narrow window for energy transmitting through is successfully opened with in a broad absorbance band. Fig. 2(b) also shows the simulated spectra of the sample. It is carried out through resorting to finite difference time domain (FDTD) method. In simulations, without loss of reality, we consider periodic boundary conditions, i.e., perfect electric (x-z plane) and perfect magnetic (y-z plane), surrounding the unit-cell and a lossy dielectric layer with the tangent of loss about 0.003. Waveguide ports are adopted to simulate TEM plane wave propagating through the medium and to collect the transmission and reflectance data. It can be seen that the experimental results agree well with the theoretical calculations, including the shape of reflectance spectrum and the transmission peak position. A little drop of peak value from 50% to 46% in experiment may be caused by the error in the fabrication process.

3 Analysis and discussion

The physical origin of the window is verified through analyzing the field distributions at the transmission peak frequency. Fig. 3(a) demonstrates the electric energy density on the x-y plane where ERR locates. It is noteworthy that an apparent coupling phenomenon is observed in the region between ERR and aperture, indicating an analo-

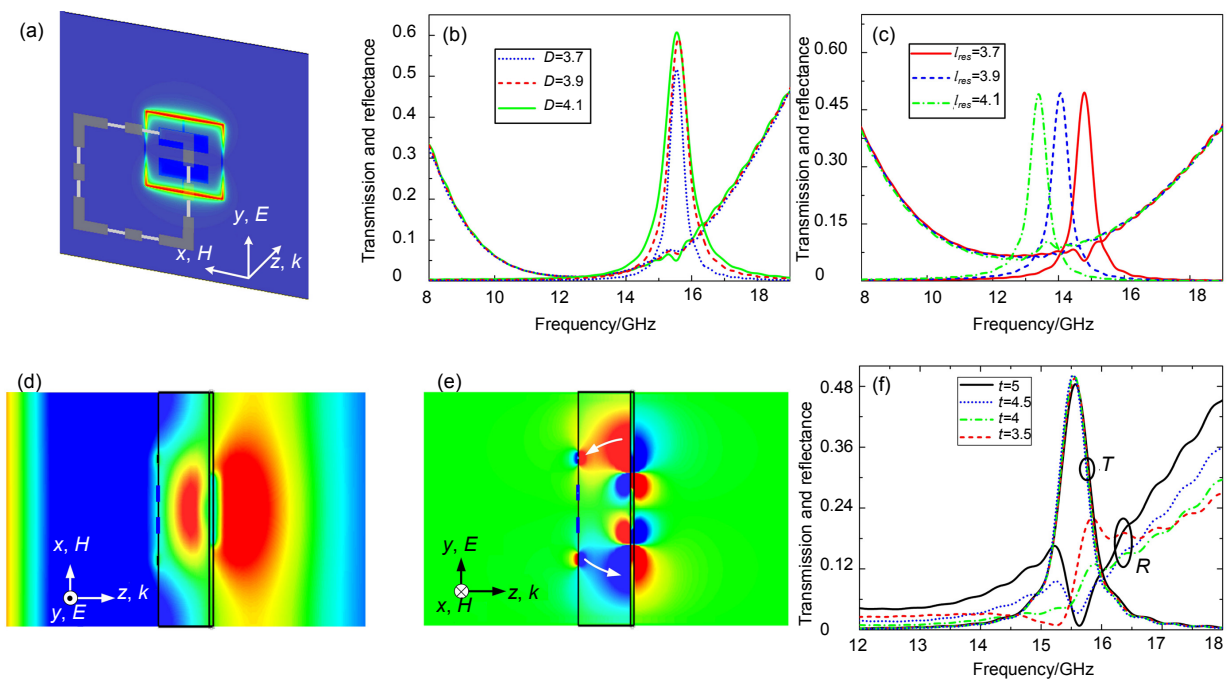

Fig.3 (a) Electric energy density at the peak frequency, the eight sticks (white) denote the inserted chip-resistors, the propagation direction is also presented. (b) and (c) Spectra with changing parameters l_{res} and D, respectively. (d) and (e) Distributions of y-component and z-component of electric field, respectively. (f) Spectra with increasing thickness t of the dielectric layer. (e) The arrows marked in the internal region indicate the direction of electric flux-lines. Red and blue colors indicate reverse phase distributions in (d) and (e).

gous dipole response for *y*-polarization. Then, we separately observe the influence of the sub-wavelength aperture and ERR on the narrow window for finding out the roles of ERR, aperture, and then figuring out the source of the dipole response. These results are shown in Figs. 3(b) and 3(c), respectively. It can be seen that the peak frequency has obvious red-shift with increasing length of ERR in *y* direction (Fig. 3(b)), while it is almost not influenced by the aperture except an observable drop of peak value when decreasing aperture size (Fig. 3(c)). These clearly clarify that the dipole resonance is excited on ERR when it interacts with the internal field. The narrowband transmission behavior can be seen as the result of a re-emission process of the captured field in the MM shelter. This kind of re-emission is induced by the dipole oscillation in ERR. While the surrounding sub-wavelength aperture only affects the re-emission efficiency by broadening or narrowing the inter-space between aperture and ERR. This is not the case of surface Plasmon[29] or frequency selective surface[30], also quite different with that proposed in Ref.[31] where the mechanism is ring-resonance induced dipole emission when a split-ring is inserted into the subwavelength aperture.

A common characteristic in Figs. 3(b) and 3(c) is that the reflectance spectra have no obvious difference and are not influenced when the dimensions of ERR and aperture change. It seems that the re-emission only directs into fore-semi-space. For detail analysis, we plot the lateral field distribution to observe the re-emission process. Fig. 3(d) shows the *y*-component of electric field in *x*-*z* plane. It is evident that the forwards-emission is normal and un-affected, while the backwards-case is completely blocked. A portion of energy emitting back is re-coupled and strong localized into the internal region between ERR and the square-loop again. This is the reason why the low-echo characteristic in the transmission window keeps almost the same with that at other frequencies as shown in Fig. 2(b). Further evidence is highlighted by the *z*-component of electric field in *y*-*z* plane in Fig. 3(e). Guided by the electric flux-lines, it clearly demonstrates the participation of the backwards-emission field into the coupling supported by ERR and the loop. This coupling strongly depends on the thickness of the MM. As depicted in Fig. 3(f), the changing of thickness does not affect the transmission peak owing to that it is mainly dominated by ERR, but weakens the ability of the coupling cavity, resulting in the deterioration of the reflectance spectra.

The performance of the MM shelter and its ability for shading electromagnetic receiver are demonstrated by carrying out a numerical experiment, including three main portions: a dipole array acting as a signal receiver, a remote point source with tunable amplitude utilized to model the far-field excitation of a signal source, and an inserted MM shelter. The results are displayed in Fig. 4. As presented in Figs. 4(a) and 4(b), the wavefront shows an obvious distortion caused by the strong scattering of the dipole array. When the MM shelter is placed in front of the dipole array and incident wave is located at the transmission peak frequency, the wavefront has little disturbance and keeps almost the same with the case that wave transmits in free space. At the same time, the coupling field of dipole array indicates that the inner detector can effectively receive signals through the window. Although one part of scattering field in the covered space may return back into the outside space through the window, it is believed that less than ten percent of the whole incident energy will escapes away because only the scattering field within about 90 degree azimuth angle can pass through and others are re-absorbed or reflected back into the covered space by shelter. Further demonstration of the invisibility performance can be obtained by comparing the wavefront at the frequency in and out of the window such as 13 GHz shown in Fig. 4(c).

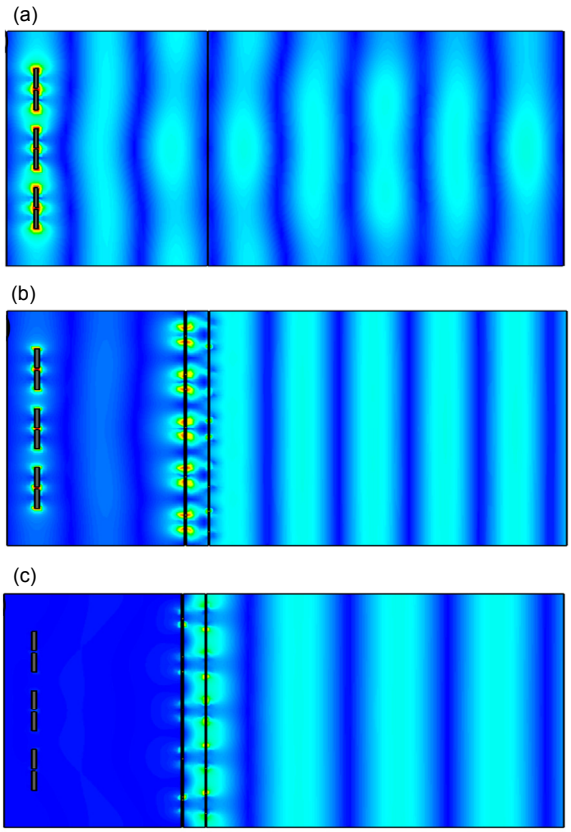

Fig.4 Demonstration of the ability of the proposed MM shelter for hiding an array of electromagnetic receiver. (a) and (b) Distribution of the wavefront in the simulated space without and with the proposed MM shelter at 15.4 GHz, respectively. (c) Distribution of the wavefront with the proposed invisibility 13 GHz. The incident wave transmits from right to left.

4 Conclusions

Hiding a detector is not a nascent topic. In antenna field, microwave engineers often use absorbing layers to construct a radome in order to reduce the radar-echo of in-

ner antenna. However, the absorbed incident wave is out of the operating band of antenna, thus having no consequential help on the reduction of antenna's in-band echo. We have designed and demonstrated a low-echo MM shelter with in-band electromagnetic narrow window. By introducing a selective re-emission mechanism of the energy captured by an absorbing layer, we observe that at least half of energy can pass through the narrow window located into the absorption band, and the broad low-echo feature is not influenced. This device is believed to be suitable for the in-band scattering reduction of antennas which are especially designed to work in the receiving mode. We expect that, the concept and design reported here will influence the future design of electromagnetic absorbers and radomes, generating a new research hot topic in electromagnetic invisibility field. Our design may be applied in wireless local area network to cancel additional multi-paths, or signal degradation because it can effectively absorb useless signals without significantly attenuating mobile phone signals.

Acknowledgements

This work is supported by the National Basic Research Program (973) of China under Grant (2013CBA 01700).

References

1 Salisbury W W. Absorbent body for electromagnetic waves: US, 2599944 [P]. 1952.

2 Luo Xiangang. Principles of electromagnetic waves in metasurfaces [J]. *Science China Physics*, *Mechanics & Astronomy*, 2015, **58**(9): 594201.

3 Luo Xiangang, Pu Mingbo, Ma Xiaoliang, *et al*. Taming the electromagnetic boundaries via metasurfaces: from theory and fabrication to functional devices[J]. *International Journal of Antennas and Propagation*, 2015, **2015**: 204127.

4 Pendry J B, Schurig D, Smith D R. Controlling electromagnetic fields[J]. *Science*, 2006, **312**(5781): 1780–1782.

5 Leonhardt U. Optical conformal mapping[J]. *Science*, 2006, **312**(5781): 1777–1780.

6 Swandic J R. Bandwidth limits and other considerations for monostatic RCS reduction by virtual Shaping[R]. West Bethesda: Naval Surface Warfare Center, Carderock Division, 2004.

7 Pu Mingbo, Zhao Zeyu, Wang Yanqin, *et al*. Spatially and spectrally engineered spin-orbit interaction for achromatic virtual shaping[J]. *Scientific Reports*, 2015, **5**: 9822.

8 Schurig D, Mock J J, Justice B J, *et al*. Metamaterial electromagnetic cloak at microwave frequencies[J]. *Science*, 2006, **314**(5801): 977–980.

9 Liang Dachuan, Gu Jianqiang, Han Jiaguang, *et al*. Robust large dimension terahertz cloaking[J]. *Advanced Materials*, 2012, **24**(7): 916–921.

10 Valentine J, Li J, Zentgraf T, *et al*. An optical cloak made of dielectrics[J]. *Nature Materials*, 2009, **8**(7): 568–571.

11 Ni Xingjie, Wong Z J, Mrejen M, *et al*. An ultrathin invisibility skin cloak for visible light[J]. *Science*, 2015, **349**(6254): 1310–1314.

12 Bliokh K Y, Rodríguez-Fortuño F J, Nori F, *et al*. Spin-orbit interactions of light[J]. *Nature Photonics*, 2015, **9**(12): 796–808.

13 Pu Mingbo, Li Xiong, Ma Xiaoliang, *et al*. Catenary optics for achromatic generation of perfect optical angular momentum[J]. *Science Advances*, 2015, **1**(9): e1500396.

14 Tang Dongliang, Wang Changtao, Zhao Zeyu, *et al*. Ultrabroadband superoscillatory lens composed by plasmonic metasurfaces for subdiffraction light focusing[J]. *Laser & Photonics Reviews*, 2015, **9**(6): 713–719.

15 Ma Xiaoliang, Pu Mingbo, Li Xiong, *et al*. A planar chiral meta-surface for optical vortex generation and focusing[J]. *Scientific Reports*, 2015, **5**: 10365.

16 Knott E F, Tulley M T, Shaeffer J F. Radar Cross Section[M]. 2nd ed. Raleigh: SciTech Publishing, 2004.

17 Alù A, Engheta N. Achieving transparency with plasmonic and metamaterial coatings[J]. *Physical Review E*, 2005, **72**(1): 016623.

18 Alù A, Engheta N. Cloaking a sensor[J]. *Physical Review Letters*, 2009, **102**(23): 233901.

19 Veselago V G. The electrodynamics of substances with simultaneously negative values of ε and μ[J]. *Soviet Physics Uspekhi*, 1968, **10**(4): 509–514.

20 Smith D R, Padilla W J, Vier D C, *et al*. Composite medium with simultaneously negative permeability and permittivity[J]. *Physical Review Letters*, 2000, **84**(18): 4184–4187.

21 Lier E, Werner D H, Scarborough C P, *et al*. An octave-bandwidth negligible-loss radiofrequency metamaterial[J]. *Nature Materials*, 2011, **10**(3): 216–222.

22 Feng Qin, Pu Mingbo, Hu Chenggang, *et al*. Engineering the dispersion of metamaterial surface for broadband infrared absorption[J]. *Optics Letters*, 2012, **37**(11): 2133–2135.

23 Pu Mingbo, Chen Po, Wang Yanqin, *et al*. Anisotropic meta-mirror for achromatic electromagnetic polarization manipulation[J]. *Applied Physics Letters*, 2013, **102**(13): 131906.

24 Grady N K, Heyes J E, Chowdhury D R, *et al*. Terahertz metamaterials for linear polarization conversion and anomalous refraction[J]. *Science*, 2013, **340**(6138): 1304–1307.

25 Guo Yinghui, Yan Lianshan, Pan Wei, *et al*. Achromatic polarization manipulation by dispersion management of anisotropic meta-mirror with dual-metasurface[J]. *Optics Express*, 2015, **23**(21): 27566–27575.

26 Pu Mingbo, Hu Chenggang, Wang Min, *et al*. Design principles for infrared wide-angle perfect absorber based on plasmonic structure[J]. *Optics Express*, 2011, **19**(18): 17413–17420.

27 Pu Mingbo, Feng Qin, Wang Min, *et al*. Ultrathin broadband nearly perfect absorber with symmetrical coherent illumination[J]. *Optics Express*, 2012, **20**(3): 2246–2254.

28 Watts C M, Liu Xianliang, Padilla W J. Metamaterial electromagnetic wave absorbers[J]. *Advanced Materials*, 2012, **24**(23): OP98–OP120.

29 Ebbesen T W, Lezec H J, Ghaemi H F, *et al*. Extraordinary optical transmission through sub-wavelength hole arrays[J]. *Nature*, 1998, **391**(6668): 667–669.

30 Munk B A. Frequency Selective Surfaces: Theory and Design[M]. New York: Wiley, 2000.

31 Yin Xiaogang, Huang Chengping, Wang Qianjin, *et al*. Transmission resonance in a composite plasmonic structure[J]. *Physical Review B*, 2009, **79**(15): 153404.